Earth and Planetary Science Letters, 76 (1985/86) 71–83
Elsevier Science Publishers B.V., Amsterdam – Printed in The Netherlands

[6]

Diagenesis and convection reflected in pore water chemistry on the western flank of the East Pacific Rise, 20 degrees south

Michael L. Bender [1], Andrew Hudson [1], David W. Graham [1,*], Ross O. Barnes [2], Margaret Leinen [1] and David Kahn [1]

[1] *Graduate School of Oceanography, University of Rhode Island, Kingston, RI 02881 (U.S.A.)*
[2] *Rosario Research, Walla Walla College, College Place, WA 99324 (U.S.A.)*

Received January 28, 1985; revised version received August 2, 1985

NO_3^-, PO_4^{3-}, SiO_2, total alkalinity (TA), Ca^{2+}, Mg^{2+} and O_2 were measured in seventeen in situ pore water profiles at 3 sites on the western flank of the East Pacific Rise at 20° S latitude. The top 1–2 m of the sediment was oxic at all sites. Stoichiometric modeling shows the C/N of the decomposing organic matter to be about 106/6.6 while C/P ranges from 106/0.7 to 106/0.25. The TA rise is greater than predicted by models assuming calcite saturation, suggesting that phases other than calcite are important in the alkalinity balance and control of $CaCO_3$ saturation.

At Site III (crustal age 4.6 Myr), anomalous pore water NO_3^- and SiO_2 profiles were observed in areas of high heat flow (and inferred upwelling of pore waters through sediments) and low heat flow (and inferred downwelling). NO_3^- and SiO_2 profiles at the high heat flow site support the heat flow evidence for upwelling; the low heat flow NO_3^- and SiO_2 profiles give equivocal evidence for downwelling. No hydrothermal Ca^{2+}, Mg^{2+}, or F^- anomalies were observed in the upwelling pore waters, suggesting the absence of significant water/rock reactions during convection at this site.

1. Introduction

Recent workers have described changes in pore water concentrations of bioreactive elements in terms of the stoichiometry of organic matter oxidation and $CaCO_3$ dissolution [1–4]. The stoichiometric models quantitatively relate the relative decrease in pore water O_2 concentrations and the increases in pore water concentrations of NO_3^-, PO_4^{3-}, TCO_2 (total CO_2), TA (total alkalinity) and other constituents through assumptions or deductions of the C : N : P : H : O ratios in the decomposing organic matter, as well as the assumption of $CaCO_3$ saturation. We report here on the pore water chemistry of sediments at 20°S on the western flank of the East Pacific Rise. The results are interpreted using stoichiometric models to infer the C/N and C/P ratios of organic matter undergoing oxidation, and the influence of metabolic CO_2 on $CaCO_3$ dissolution.

The heat balance of mid-ocean ridge flanks can be reconciled only by invoking extensive seawater circulation through the crust [5]. In several recent studies, pore water profiles have been interpreted as reflecting convection through ridge flank sediments [6–8], during recharge or discharge of the basement aquifer. Evidence from bathymetry and heat flow studies suggest that advection of pore waters through the sediments is occurring at our study site on 4.6 Myr old crust (Site III). We outline the geophysical evidence for convection, and show how convection is also reflected in pore water nutrient profiles at this site.

2. Experimental methods

Sampling was done aboard the R/V "Thomas Washington" during Leg II of the Ariadne expedition in February–April, 1982. The context of the study sites (Table 1 for hydrothermal activity was established by transponder navigated Seabeam mapping, heat flow determinations, and gravity coring [9,10]. Pore waters were collected using two in-situ samplers: the multisampler of R.O. Barnes and a derivative URI instrument. Barnes' sampler

* Present address: Woods Hole Oceanographic Institution, Woods Hole, Mass., U.S.A.

0012-821X/85/$03.30

TABLE 1

Ariadne Leg II study sites

Harpoon	Latitude, longitude	Depth (m)
Site II (crustal age = 7.8 Myr)		
3	19°24′16″S, 119°50′35″W	3590
4	19°23′41″S, 119°54′00″W	3710
7	19°24′03″S, 119°47′25″W	3565
8	19°24′32″S, 119°53′06″W	3685
9	19°24′18″S, 119°47′24″W	3565
Site III (crustal age = 4.6 Myr)		
10	18°54′31″S, 116°50′24″W	3425
11	18°54′58″S, 116°51′54″W	3432
13	18°55′21″S, 115°49′56″W	3335
14	18°55′20″S, 116°49′39″W	3335
15	18°55′19″S, 116°49′52″W	3335
16	18°53′59″S, 116°55′06″W	3550
Site IV (crustal age = 2.5 Myr)		
17	19°29′37″S, 114°57′44″W	3435
18	19°29′16″S, 114°57′10″W	3382
19	19°29′40″S, 114°55′54″W	3390
20	19°29′34″S, 114°58′34″W	3410
21	19°29′38″S, 114°57′45″W	3435
22	19°29′33″S, 114°59′06″W	3365

has two probes (one 210 cm and one 45 cm long) which, during penetration, seat simultaneously in the sediment. During sampling, a valve is opened creating a 400 psi pressure differential between the outside of the probe and various sampling coils. This pressure differential drives pore waters through filters, into tubing attached to ports in the probes, and into sampling tubes. Up to 20 pore water samples may be collected on each deployment, depending on the penetration depth of the probe(s). On the Barnes sampler, or "harpoon", the probe, filters, capillary tubing of the sampling train which collects pore waters, and the check valves are all stainless steel; the sample coils are made of nylon. These materials clearly contaminate samples for Mn, Fe and other trace metals; PO_4^{3-} is contaminated as well (reflected by considerable scatter in the data). Results of analyses on samples collected by ports which did not penetrate into the sediment were similar to those for bottom waters collected by hydrocasts at these sites for the major ions Cl^-, Ca^{2+}, and Mg^{2+} as well as for O_2, SiO_2, NO_3^-, and total alkalinity (Table 2). We conclude that contamination with respect to these species is not a problem in the Barnes sampler.

The URI sampler is different in several respects. It contains a single 1 m long Ti probe with 20 sampling ports and no check valves. Sampling materials include polyethylene fittings, sampling coils, and sampling tubes. During the cruise we used both teflon-coated and uncoated stainless steel unions for joining the components of the sampling line. We found that samples drawn into ports using teflon-coated hardware were not contaminated for PO_4^{3-}, while those samples contacting uncoated stainless steel showed more scatter in PO_4^{3-}. With regard to all other species reported on here (except O_2), results for ports not penetrat-

TABLE 2

Concentrations ($\pm 1\sigma$) of NO_3^-, SiO_2, Ca^{2+}, TA and O_2 in all samples from Barnes and URI harpoon ports which did not penetrate into the sediment, compared with bottom water concentrations. Data for URI ports with coated and uncoated stainless steel fittings in the sampling train are given separately. Average fractions of deionized water in the sample are given in the last column. $\Delta[PO_4^{3-}]$ measured on samples from the Barnes harpoon and the ports of the URI harpoon with bare stainless steel fittings are erratic and not reported. $\Delta[O_2]$ are corrected for contamination as described in the text

Harpoon type	NO_3^- (μmol/kg)	SiO_2 (μmol/kg)	PO_4^{3-} (μmol/kg)	Ca^{2+} mmol/kg	TA (meq/kg)	(O_2) (μmol/kg)	%D.I. dilution
Barnes	36.6 ± 0.5	128 ± 3		10.26 ± 0.15	2.389 ± 0.029	165 ± 7	1.0 ± 0.6
	$n = 52$	$n = 69$		$n = 39$	$n = 13$	$n = 14$	$n = 33$
URI	36.4 ± 0.4	127 ± 3	2.47 ± 0.07	10.24 ± 0.16	2.389 ± 0.031		
(teflon)	$n = 36$	$n = 34$	$n = 29$	$n = 14$	$n = 20$		
URI	36.3 ± 0.6	126 ± 3		10.24 ± 0.13	2.407 ± 0.029		
(uncoated)	$n = 29$	$n = 29$		$n = 18$	$n = 15$		
URI	36.4 ± 0.5	127 ± 3	2.47 ± 0.07	10.24 ± 0.14	2.404 ± 0.032	–	1.3 ± 0.7
(total)	$n = 65$	$n = 63$	$n = 29$	$n = 32$	$n = 35$	–	$n = 72$
Niskin bottom water	36.2 ± 0.6	127 ± 2	2.47 ± 0.12	10.27 ± 0.03	2.377 ± 0.026	165 ± 5	
	$n = 19$	$n = 21$	$n = 21$	$n = 13$	$n = 6$	$n = 5$	

ing sediments were similar to bottom water values (Table 2), indicating that contamination for the species is insignificant. O_2 concentrations in samples collected with the URI harpoon were anomalously high because of diffusion of O_2 through permeable plastics. Thus, where O_2 data is reported, it is from the Barnes harpoon, while PO_4^{3-} data is reported only from the teflon-coated samplers in the URI instrument.

All samples were drawn within 1 hour of coming on-deck. Where O_2 analyses were performed, samples were drawn directly from the harpoon and immediately "pickled". All other samples were drawn ito precleaned 25 ml polyethylene syringes and filtered through precleaned 25 mm, 0.4 μm Nuclepore filters.

Since sampling probes did not completely penetrate into the mud, absolute depths of our samples with respect to the sediment-water interface must be estimated from the observed pore water profiles themselves. We have estimated depths assuming that below the interface $[NO_3^-]$ and $[SiO_2]$ rise asymptotically with depth according to the equation:

$$\Delta C_z = (C_\infty - C_0)(1 - e^{-\alpha z}) \quad (1)$$

where ΔC_z is the concentration increases above the bottom water value, C_∞ and C_0 are, respectively, the asymptotic and bottom water concentrations, α is the reciprocal of the e-folding distance for the concentration increase, and z is depth below the sediment-water interface. The position of the sediment-water interface was then determined by extrapolating up to the depth where the calculated pore water value equals the bottom water value. The uncertainty is about ± 2 cm.

The other important source of uncertainty introduced by sampling results from leakage of bottom water down the sides of the harpoon probe. If the probe does not seat perfectly in the sediment, subsurface samples may include a component of bottom water that has channeled down the probe. Such dilution would make pore water concentration gradients appear less steep than the true gradients, and therefore affect kinetic modeling. However, it would not affect the interpretation of pore water changes in NO_3^-, PO_4^{3-} and O_2 in terms of the stoichiometric models, since concentrations of these constituents vary as linear mixtures of bottom water and asymptotic pore water.

Shipboard chemical analyses were done as follows: SiO_2, NO_3^- and PO_4^{3-} by colorimetric analysis using an autoanalyzer; O_2 by Winkler titration; total alkalinity by Gran titration using the extended calculations method of Hanson and Jagner [11]; Ca^{2+} and Mg^{2+} by complexometric EGTA/EDTA titrations, respectively [12,13]; F^- by colorimetry [14] and Cl^- by Mohr titration. SiO_2, NO_3^- and PO_4^{3-} analyses are reported with respect to the bottom water value, rather than as absolute concentrations, as this approach improves precision by eliminating blank uncertainties in the autoanalyzer determinations.

All measured pore water concentrations (Table 3A, B, C) were corrected for dilution with the deionized water used to fill the sampling coils of the harpoons. In about one-half of the samples, this correction was made directly from the measured chlorinity of each sample, introducing an uncertainty equal to the precision of the chloride analysis ($\pm 0.3\%$). In the other samples, the concentrations were corrected by the average measured dilution ($1.3 \pm 0.7\%$ for the URI harpoon and $1.0 \pm 0.6\%$ for the Barnes harpoon; Table 2),

TABLE 3A
Pore water data for Site II

AR2-II-3 (URI harpoon)

Depth (cm)	ΔNO_3^- (μmol/kg)	ΔSiO_2 (μmol/kg)	ΔPO_4^{3-} (μmol/kg)	TA (meq/kg)
0	0	0	0	2.369
2.5	0.9	4		2.452
11.5	2.0	12		2.561
16.5	2.0	13	0.17	2.484
21.5	1.8	13		2.470
31.5	2.8	17		2.578
36.5	2.2	13	0.13	2.468
41.5	3.4	22		2.613
51.5	2.4	13		2.568
66.5	4.1	21	0.22	2.580
71.5	3.4	14		2.535
81.5	3.9	17		2.537

AR2-II-4 (Barnes harpoon)

Depth (cm)	ΔSiO_2 (μmol/kg)
1.6	5
41.6	38
81.6	39
121.6	41

AR2-II-7 (URI harpoon)

Depth (cm)	ΔNO_3^- (μmol/kg)	ΔSiO_2 (μmol/kg)	ΔPO_4^{3-} (μmol/kg)	TA (meq/kg)
1.9	0.3	2		2.423
5.9	0.9	8	0.61	2.475
10.9	1.3	12		2.521
15.9	2.0	16	0.32	2.527
20.9	2.6	19		2.554
25.9	2.6	18	0.20	2.619
30.9	2.7	20		2.568
35.9	2.6	25	0.69	2.692
40.9	2.5	19		2.545
45.9	2.9	21	0.29	2.587
50.9	3.8	30		2.666
55.9	2.9	26	0.10	2.611
65.9	3.7	33	0.37	2.766
70.9	3.3	31		2.718
75.9	3.7	31	0.56	2.687
80.9	3.5	25		2.590
90.9	3.5			2.556

AR2-II-8 (Barnes harpoon)

Depth (cm)	ΔNO_3^- (μmol/kg)	O_2 (μmol/kg)	ΔSiO_2 (μmol/kg)	TA (meq/kg)
5	0.8	159	7	
10.9	1.6	136	21	2.627
11	1.4	141	13	
30.9	2.6	137	24	2.700
70.9	4.1	124	41	2.802
110.9	4.6	122	31	2.791
130.9	4.5	108	31	2.753

AR2-II-9 (Barnes harpoon)

Depth (cm)	ΔNO_3^- (μmol/kg)	ΔSiO_2 (μmol/kg)	TA (meq/kg)
8.5	0.8	6	2.472
9.3	1.7	14	2.658
14.3	2.4	16	2.687
20.3	2.6	17	2.637
28.5	2.6	15	2.643
48.5	3.6	20	2.664
68.5	4.3	27	2.765
88.5	4.4	27	2.718
108.5	4.5	32	2.852
128.5	5.3	31	2.745
148.5	5.3	32	2.859
168.5	5.2	30	2.742

introducing a somewhat larger uncertainty.

The sampling and analytical blanks for O_2, and the overall analytical uncertainty, were determined empirically by analyzing bottom water from Barnes harpoon ports which did not penetrate the sedi-

TABLE 3B

Pore water data for Site III

AR2-III-10 (Barnes harpoon)

Depth (cm)	ΔNO_3^- (μmol/kg)	O_2 (μmol/kg)	ΔSiO_2 (μmol/kg)	TA (meq/kg)
3.3	0.3	152	9	2.485
5.8	0.2	163	11	
13.3				2.626
15.6	0.9		17	
18.3	2.0		26	
24.3	3.1	133	23	
35.6	2.7	133	26	2.656
55.6	4.2		34	2.726
75.6	4.7	113	38	2.723
95.6	5.0		40	2.672
115.6	5.6	96	43	2.718
135.6	6.2		44	2.716
155.6	6.0	91	45	2.707
175.6	5.0		46	2.664

AR2-III-11 (URI harpoon)

Depth (cm)	ΔNO_3^- (μmol/kg)	ΔSiO_2 (μmol/kg)	ΔPO_4^{3-} (μmol/kg)	TA (meq/kg)
2.6	1.0	9		
6.6	2.0	16	0.37	
11.6	2.7	20		2.563
16.6	0.8	3	0.02	
21.6	3.1	22		2.572
31.6	3.7	24		2.595
36.6	3.2	25	0.41	2.552
41.6	4.4	28		2.596
46.6	4.8	34	0.45	2.612
51.6	4.6	34		2.601
56.6	4.4	34	0.41	2.634
66.6	4.4	33	0.42	2.608
71.6	5.2	33		2.640
76.6	5.8	34	0.58	2.631
81.6	5.8	30		2.622
91.6	6.1	35	0.48	2.643

AR2-III-13 (Barnes harpoon)

Depth (cm)	ΔNO_3^- (μmol/kg)	ΔSiO_2 (μmol/kg)	TA (meq/kg)
3		3	
8	1.2	29	2.585
13.4	1.0	23	2.575
18	1.3	46	2.554
23	1.9	48	2.599
29	2.2	54	2.527
33.4	1.9	50	2.570
53.4	1.6	60	2.547
73.4	1.3	62	2.524
93.4	1.3	64	2.490
113.4	3.7	67	2.592
133.4	1.3	73	2.636
153.4	0.6	78	2.588

AR2-III-14 (URI harpoon)

Depth (cm)	ΔNO_3^- (μmol/kg)	ΔSiO_2 (μmol/kg)	ΔPO_4^{3-} (μmol/kg)	TA (meq/kg)
3.1	0.9	10		
8.1	1.4	12	0.16	2.532
13.1	1.4	17		
18.1	2.1	20	0.24	2.530
23.1	3.1	22		
28.1	2.7	25	0.28	2.573
33.1	3.6	27		
38.1	3.8	30	0.31	2.678
43.1	3.6	27		
48.1	3.4	28	0.29	2.623
58.1	4.1	33	0.35	2.669
63.1	3.4	24		
68.1	3.8	32	0.29	2.630
73.1	4.2	34		
83.1	3.9	32	0.28	2.608

AR2-III-15 (Barnes harpoon)

Depth (cm)	ΔNO_3^- (μmol/kg)	ΔSiO_2 (μmol/kg)	TA (meq/kg)
5.9	0.8	16	2.424
5.9	0.5	7	2.473
25.9	1.2	25	2.524
45.9	1.8	55	2.539
65.9	1.4	67	2.474
85.9	1.4	64	2.495
105.9	1.2	64	2.485
125.9	1.9	68	2.465
145.9	0.9	64	2.448

AR2-III-16 (URI harpoon)

Depth (cm)	ΔNO_3^- (μmol/kg)	ΔSiO_2 (μmol/kg)	ΔPO_4^{3-} (μmol/kg)
0.3	0.4	3	
5.3	1.5	10	0.37
10.3	2.2	15	
15.3	3.4	20	0.37
20.3	2.6	14	
25.3	3.3	20	0.35
35.3	2.8	19	0.36
40.3	2.9	20	
45.3	3.2	20	0.46
50.3	2.8	19	
60.3	3.5	20	0.43

ment. The average uncorrected $[O_2]$ of these samples was 178 ± 4 μmol/kg, compared with a bottom water $[O_2] = 165$ μmol/kg as measured in water collected using a Niskin bottle, and noted in other investigations of the area [15]. The total blank was therefore assumed to be 13 μmol/kg

TABLE 3C

Pore water data for Site IV

AR2-IV-17 (Barnes harpoon)

Depth (cm)	ΔNO_3^- (μmol/kg)	O_2 (μmol/kg)	ΔSiO_2 (μmol/kg)	TA (meq/kg)
4.4	1.2		8	2.486
5.3	1.4		13	2.551
9.4	2.4	136	25	2.658
15.5	2.3	128	25	
19.4	3.4		30	2.739
24.4	3.8		34	2.739
25.3	3.2		28	2.678
30.4	3.9	125	35	
45.3	4.5	120	37	
65.3	5.4		42	2.766
85.3	5.8	104	45	
105.3	6.3		50	2.828
125.3	6.2	96	54	
145.3	6.2		60	2.862
165.3	6.9	83	65	
185.3	6.6		62	2.849

AR-IV-18 (URI harpoon)

Depth (cm)	ΔNO_3^- (μmol/kg)	ΔSiO_2 (μmol/kg)	ΔPO_4^{3-} (μmol/kg)	TA (meq/kg)
2.6	0.4	6	0.31	2.430
7.6	0.8	8		
12.6	2.0	13	0.60	2.553
17.6	2.5	20		
22.6	2.9	21	0.81	2.581
27.6	3.2	21		
32.6	3.1	24	0.69	2.594
37.6	3.1	23		
42.6	3.0	25	0.92	2.581
52.6	3.4	27	0.96	2.610
57.6	3.2	27		
62.6	3.5	25	1.00	2.618
67.6	3.7	27		
77.6	4.0	30	0.98	2.597

AR2-IV-19 (URI harpoon)

Depth (cm)	ΔNO_3^- (μmol/kg)	ΔSiO_2 (μmol/kg)	ΔPO_4^{3-} (μmol/kg)	TA (meq/kg)
0.6		3		2.465
2.6	0.1	9	0.34	2.467
4.6	0.6	9		
8.6	0.8	12	0.48	2.460
13.6	1.0	12		
18.6	1.8	13	0.41	2.522
23.6	1.5	14		
28.6	1.9	15	0.67	2.517
33.6	2.5	20		
38.6	2.0	15	0.78	2.507
43.6	2.8	16		

TABLE 3C (continued)

Depth (cm)	ΔNO_3^- (μmol/kg)	O_2 (μmol/kg)	ΔSiO_2 (μmol/kg)	TA (meq/kg)
48.6	2.8	25	0.72	2.569
53.6	2.7	17		
58.6	2.6	25	0.80	2.522
68.6	2.8	19	0.82	2.545
73.6	3.0	15		
78.6	2.5	20	0.92	2.574
83.6	2.8	26		
93.6	3.4	23	0.84	2.549

AR2-IV-20 (URI harpoon)

Depth (cm)	ΔNO_3^- (μmol/kg)	ΔSiO_2 (μmol/kg)	ΔPO_4^{3-} (μmol/kg)	TA (meq/kg)
1.2	0.2	10	0.02	2.393
3.2	0.3	12		
7.2	0.7	24	0.39	2.443
12.2	2.2	28		
17.2	2.5	28	0.63	2.524
22.2	2.4	28		
27.2	2.5	28	0.83	2.517
32.2	2.7	28		
37.2	2.5	28	0.89	2.520
42.2	3.0	28		
47.2	3.1	26	0.84	2.592
52.2	2.4	28		
57.2	3.2	28	0.99	2.565
67.2	3.5	24	0.93	2.553
72.2	3.3	26		
77.2	2.4	30	1.09	2.552
82.2	3.7	33		
92.2	3.6	35	0.92	2.549

AR2-IV-21 (URI harpoon)

Depth (cm)	ΔNO_3^- (μmol/kg)	ΔSiO_2 (μmol/kg)	ΔPO_4^{3-} (μmol/kg)	TA (meq/kg)
2.6	0.9	7	0.53	2.484
7.6	2.1	16		2.569
12.6	2.4	20	0.92	2.577
17.6	3.3	29		2.600
22.6	3.6	30	1.11	2.589
27.6	4.0	27		
32.6	4.4	31	0.96	2.684
37.6	4.2	28		
42.6	5.1	38	1.27	2.716
47.6	4.2	33		
52.6	4.2	38	1.14	2.656
57.6	4.8	40		
62.6	4.5	39	1.32	2.663
67.6	4.3	39		2.656
77.6	5.1	41	1.23	2.670

AR2-IV-22 (Barnes harpoon)

Depth (cm)	ΔNO_3^- (μmol/kg)	ΔSiO_2 (μmol/kg)
2		9
8	1.8	9
16.5	2.3	19
18.9	1.3	14
21.5	2.3	19
31.5	2.9	16
36.5	3.5	26
38.9	3.8	23
42.5	3.3	22
58.9	4.6	30
78.9	5.0	35
98.9	4.6	33
118.9	4.4	36
138.9	4.2	45

and this correction was made for all pore water samples.

Overall uncertainties (± 1 std. dev.) in the difference between pore water and bottom water nutrient concentrations are estimated to be ± 3 μmol/kg for SiO_2, ± 8 μmol/kg for NO_3^-, ± 0.10 μmol/kg for PO_4^{3-}, ± 0.15 mmol/kg for Ca^{2+}, ± 0.4 mmol/kg for Mg^{2+}, ± 6 μmol/kg for O_2 and ± 30 μeq/kg for TA.

3. Stoichiometric modeling of organic matter degradation

Stoichiometric models have provided a quantitative tool for understanding the changes in pelagic sediment pore water chemistry resulting from oxidation of organic matter, as well as $CaCO_3$ dissolution driven by metabolic acids [1–4,16]. In this paper we apply this approach to extend our understanding of nutrient regeneration in oxic marine sediments, and to provide a context for evaluating evidence for advection of pore fluids.

Organic matter oxidation may be described by the following reaction:

$$(CH_2O)_{106}(NH_3)_x(H_3PO_4)_y + (106 + 2x)O_2 \rightarrow 106CO_2 + xHNO_3 + yH_3PO_4 + (106 + x)H_2O \quad (2)$$

This reaction produces sympathetic changes in pore water $[O_2]$, $[NO_3^-]$ and $[PO_4^{3-}]$ according to

the equations:

$$\frac{d[NO_3^-]}{d[O_2]} = \frac{-D(O_2)}{D(NO_3^-)} \frac{x}{(106+2x)} \quad (3)$$

$$\frac{d[PO_4^{3-}]}{d[NO_3^-]} = \frac{D(NO_3^-)}{D(PO_4^{3-})} \frac{y}{x} \quad (4)$$

$$\frac{d[PO_4^{3-}]}{d[O_2]} = \frac{-D(O_2)}{D(PO_4^{3-})} \frac{y}{(106+2x)} = \frac{d[PO_4^{3-}]}{d[NO_3^-]} \frac{d[NO_3^-]}{d[O_2]} \quad (5)$$

where D is the diffusion coefficient. Ratios of diffusion coefficients calculated using diffusivities in deionized water [17,18] are: $D(O_2)/D(NO_3^-) = 1.21$, $D(NO_3^-)/D(HPO_4^{2-}) = 2.59$, $D(NO_3^-)/D(HCO_3^-) = 1.61$. The C/N and C/P ratios of the decomposing organic matter are $106/x$ and $106/y$, respectively.

The reaction described in equation (2) changes total alkalinity, because the metabolic acids CO_2 and HNO_3 dissolve $CaCO_3$ [2–4]. For a solution at saturation with respect to $CaCO_3$, the reaction is:

$$106CO_2 + xHNO_3 + (106+x)CaCO_3 + (106+x)H_2O \rightarrow (212+x)HCO_3^- + xNO_3^- + (106+x)Ca^{2+} \quad (6)$$

The overall general reaction for organic matter oxidation and $CaCO_3$ dissolution in the oxic zone of sediments is the sum of (2) + (6);

$$(CH_2O)_{106}(NH_3)_x(H_3PO_4)_y + (106+2x)O_2 + (106+x)CaCO_3 \rightarrow (212+x)HCO_3^- + xNO_3^- + yH_3PO_4 + (106+x)H_2O + (106+x)Ca^{2+} \quad (7)$$

According to equation (7):

$$\frac{d[TA]}{d[NO_3^-]} = \frac{D(NO_3^-)}{D(TA)} \frac{(212+x)}{x} \quad (8)$$

With this background, we can interpret our results in terms of the stoichiometric model. In Fig. 1, $[O_2]$ is plotted vs. $\Delta[NO_3^-]$. The data for three harpoons (one from each site) in which O_2 was measured fall on a single line with a slope $d[O_2]/d[NO_3^-] = -11.6$ (best fit constrained to pass through bottom water concentrations), corresponding to a C/N value of 106/6.6. This ratio is

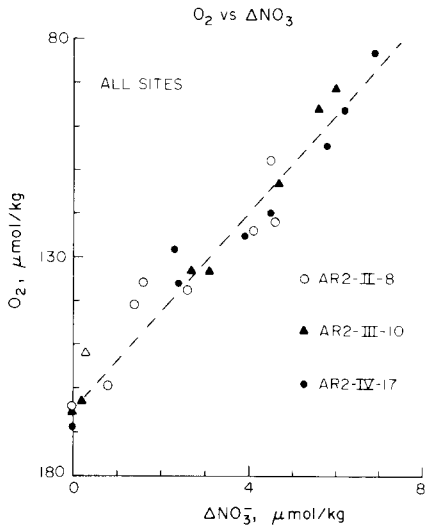

Fig. 1. $[O_2]$ vs. $\Delta[NO_3^-]$ (difference between pore water and bottom water NO_3^- concentrations) from one harpoon at each of the three study sites. Harpoon number system: AR2 (Adriadne Leg 2) + site number + harpoon number. For example, AR2-II-8 refers to Site II, HP 8.

significantly less than both the Redfield ratio (106/16) and the value for decomposing organic matter in suboxic equatorial Pacific and Atlantic sediments inferred from pore water data [16]. It is also less than the value of 106/12 inferred from pore water O_2, CO_2 and NO_3^- concentrations in oxic equatorial and subequatorial Pacific sediments [3]. Perhaps the very high C/N ratio of the decomposing organic matter at our sites is due to the extremely oligotrophic character of the overlying surface waters, with nearly complete organic C oxidation (and preferential oxidation of N-rich

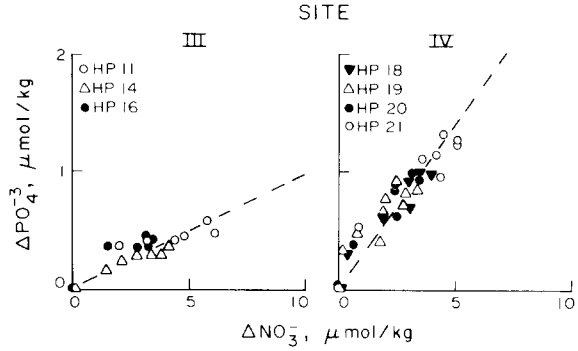

Fig. 2. $\Delta[NO_3^-]$ vs. $\Delta[PO_4^{3-}]$ for pore water profiles from Site III and Site IV.

organics within the water column) leading to a residue of N-poor sedimentary organic C.

$\Delta[PO_4^{3-}]$ is plotted vs. $\Delta[NO_3^-]$ in Fig. 2. Omitted from this plot and the ensuing discussion are data for HP 13, 15 and 16 (Site III), as these profiles are believed to be distorted by convection (see below). The data for three harpoons from Site II and four harpoons form Site IV give clear results and define curves with very different slopes: $d[PO_4^{3-}]/d[NO_3^-] = 1/10.1$ and $1/3.6$ for Sites III and IV respectively (best fits constrained to pass through bottom water concentrations). These slopes correspond to C/P values of 106/0.24 (Site III) and 106/0.7 (Site IV). The large difference between sites is unexpected. One possible explanation is solid phase uptake of diagenetic PO_4^{3-} at site III. However, while the metalliferous ferromanganese oxyhydroxides found in EPR flank sediments are certainly capable of PO_4^{3-} uptake [19,20] such uptake would likely be more extensive at Site IV, which is closer to the ridge crest and has a higher concentration of the metalliferous component [10,21].

The TA increase below the depth of $CaCO_3$ saturation predicted from the NO_3^- increase and equation (8) is $0.92 \times 1.61 \times 33.1 = 49.1$ μeq alkalinity per μmol NO_3. The factor of 0.92 enters because not all CO_2 produced by organic matter reacts with $CaCO_3$, and reaction (6) does not go to completion [4]. The observed TA-ΔNO_3^- slope may be compared with this value assuming pore water saturation with respect to either calcite or aragonite. Calcite is very slightly supersaturated (3–8 μmol/kg) in seawater at the depth and location of our cores [22], so that the modified stoichiometric model with calcite saturation predicts that TA will increase with NO_3^- from slightly below the bottom water value, and with the above slope. With respect to aragonite, bottom water at our sites is undersaturated [22]. If aragonite saturation controls pore water CO_3^{2-} chemistry, TA will rise by about 140 μeq/kg immediately below the sediment-water interface (calculated using K'_{sp} (1 atm) of Mucci [23], and depth dependence of Millero [24]). Below the interface TA would increase with NO_3^- according to the slope indicated above.

Pore water TA values are everywhere greater than predicted by the stoichiometric model, after invoking the assumption of calcite saturation (Fig. 3) (again, presumed convective profiles are omitted). At both Sites III and IV, nearly all the data fall between the calcite and aragonite saturation lines. (At Site II, TA values rise above the limit permitted for aragonite saturation, although concentration-depth profiles at this site show considerable scatter, and the results may not be as reliable as those at other sites.) One possible cause for TA values greater than those predicted by stoichiometry with calcite saturation is dissolution of aragonite within the sedimentary column. The carbonate flux associated with the "excess" TA is small, and could be supplied by burial of a few weight percent of aragonite below the sedimentary mixed layer. However X-ray diffraction analysis did not show the presence of any detectable aragonite in the sediments (quantities of 1–2 wt.% would be detected easily).

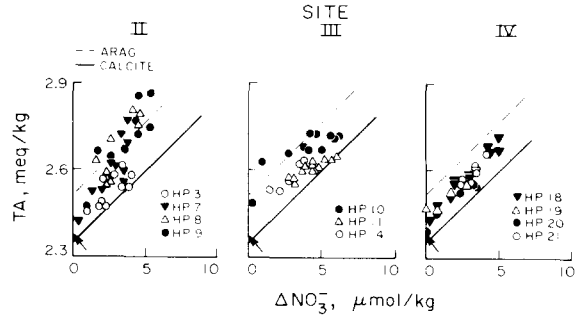

Fig. 3. TA vs. $\Delta[NO_3^-]$ for pore water profiles from Sites II, III and IV. Aragonite and calcite saturation lines plotted using K'_{sp} of Mucci [23], depth dependence of Millero [24], and slope calculated in equation (8). Plotted bottom water value is average TA measured in bottom water collected by hydrocast at site.

Other factors which may contribute to alkalinities in excess of values predicted by our calcite saturation model include unrecognized sampling artifacts, control of $CaCO_3$ solubility by some unrecognized surface phase, and the occurrence of other reactions (such as those involving aluminosilicate) which produce or consume alkalinity. It is quite possible that the processes producing the excess TA are similar to the uncharacterized reactions responsible for negative pore water concentration anomalies of K^+ and Mg^{2+} observed by Sayles [25]. Dilution of pore waters with bottom water during in situ sampling would merely move data points towards the bottom water value in Fig. 3, and could not produce the observed anomalies.

4. Rates of organic matter decomposition

The nitrification rates and SiO_2 regeneration rates at our sites can be estimated by interpreting the depth profiles in terms of the 1-layer kinetic model of Goloway and Bender [16]. The rates calculated have a considerable uncertainty, because of the possibility of channeling of bottom water down the probe, and should be regarded only as lower limits because such leakage would lower nutrient concentrations and hence concentration gradients. The rates thus calculated from our data are quite consistent, averaging 0.023 ± 0.007 ($n = 10$) μmol/cm^2 yr for the NO_3^- production rate, and 0.37 ± 0.12 μmol/cm^2 yr for the C_{org} oxidation rate (calculated assuming a C/N of 106/6.6). Data from HP 13, 15, and 16 are omitted in the averaging, as these profiles are believed to be distorted by convection. The fluxes given above were calculated from the product of the diffusivity and concentration gradient at the sediment-water interface, using the equation, $\text{Flux} = \Delta C_\infty D_a \alpha$, where ΔC_∞ is the increase in pore water concentration above the bottom water value and D_a = the apparent diffusion coefficient [17]. α is as defined for equation (1). D_a is taken as 4×10^{-6} cm^2/s for NO_3^- and 2.1×10^{-6} cm^2/s for SiO_2 [16,26]. The SiO_2 diffusion coefficient is calculated by correcting the seawater value [18] using parameters for temperature, porosity, and tortuosity effects identical to those used for correcting the NO_3^- diffusivity.

The calculated value for the C_{org} oxidation rate (0.37) may be compared with the value of 1.5 μmol/cm^2 yr for the organic carbon oxidation rate at 10°N, 140°W (MANOP site S: [16]) and values of 5–30 μmol/cm^2 yr at 140°W and 1°N (MANOP site C: [16,27,28]). The East Pacific Rise flank NO_3^- benthic fluxes reported here, along with the O_2 consumption rates and organic carbon oxidation rates calculated from them, are presently the lowest estimates for open ocean areas (see Grundmanis et al. [3]), apparently reflecting the highly oligotrophic nature of the overlying surface waters. However, the possibility remains that the low apparent rates may be an artifact of bottom water leakage down the side of the probe during sampling, as discussed above.

5. Evidence for advection at Site III

At Site III (on 4.6 myr old crust) the heat flow survey showed that several localized areas had extremely high heat flow values [9] (Fig. 4). Site III is bounded on the east by an abyssal hill ridge which trends about 010°. The ridge is highest (about 100 m) and broadest at the southern margin of the area, losing elevation and becoming narrower to the north. Along the western margin of the area is a trough about 100 m deep, the eastern edge of which is a scarp. Between the ridge and trough is a fairly flat plateau. Airgun records and coring [10] suggest that the western trough has only a very thin (< 3 m), perhaps discontinuous, sediment cover. The plateau is covered by uniform blanket of 20–25 m of pelagic sediment which thins over the abyssal hill ridge [10]. The airgun and 3.5 kHz acoustic records do not show any sediment cover on the ridge, but all cores taken on the ridge have recovered sediment. A case taken at the location of the highest heat flow value re-

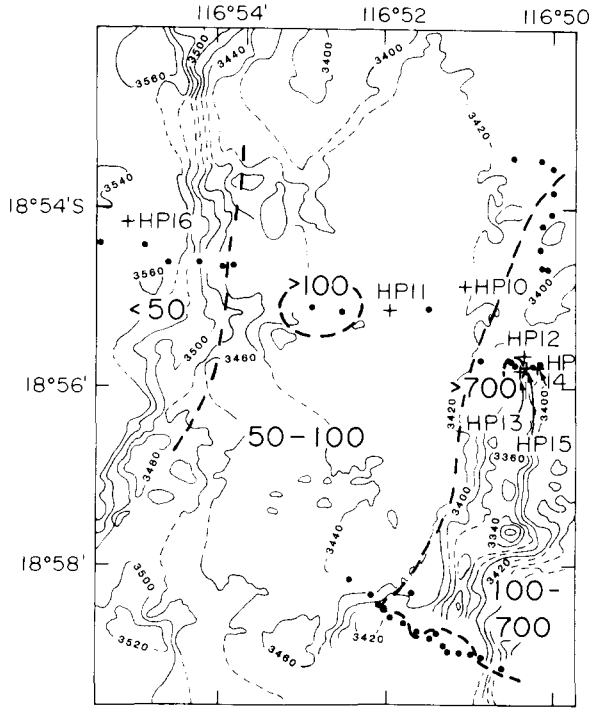

Fig. 4. Bathymetry and heat flow [5] at Site III. Light solid lines = depth contours in meters; heavy dashed lines = heat flow contours; ● = heat flow station; + = harpoon station. Heat flow is shown by the heavy numerals, in units of W/m^2.

covered 12 m of sediment with a thin layer of chalk in the core catcher [10]. High heat flow values were measured only on the flanks of the abyssal hill ridge. Heat flow at the northern end of the ridge (sites of HP 13 and 15) was > 700 mW/m^2, about three times the theoretical value for crust of this age; heat flow at the southern end of the ridge was > 400 mW/m^2 [9]. Anomalously low heat flow values averaging 20 mW/m^2 [9] were present in the trough at the western margin of the area (site of HP 16). The heat flow and sediment data suggest downwelling at the exposed scarp and thinly covered through in the west and upwelling along the covered ridge in the east. The sediments covering the ridge consist of nannofossil ooze with about 20% fine-grained clays and iron oxides. There is no evidence of high-temperature minerals, thermal diagenesis, or extensive dissolution of the calcareous microfossils in the sediments [10].

Two lines of chemical evidence may suggest pore water advection in sediments: (1) pore water concentration anomalies of major ions or other biounlimited elements which are too large to have been produced by diagenesis, and which change asymptotically (suggesting convection) rather than linearly (suggesting diffusion) with depth, and (2) diagnostic anomalies in pore water nutrient profiles. In the following discussion, we analyze the Site III nutrient profiles in terms of a diffusion-reaction-advection model, and examine whether pore water data are consistent with heat flow evidence for advection. Assuming an exponentially decreasing production rate with depth for NO_3^- and SiO_2, and assuming steady state and constant diffusivity with depth, the diffusion-advection-reaction equation is:

$$\frac{dC}{dt} = D_a \frac{d^2C}{dz^2} + w\frac{dC}{dz} + J_0 e^{-\alpha z} = 0 \qquad (9)$$

where C = concentration, t = time, D_a = apparent pore water diffusion coefficient (incorporating tortuosity and porosity effects), w = advection rate (positive upward), z = depth, α = reciprocal of the e-folding distance for decrease in production, and J_0 = production rate at the sediment-water interface. In this equation, it is assumed that reaction rate decreases exponentially with depth. Given the boundary conditions $C(z=0) = C_0$, $C(z=\infty) = C_\infty$, and taking $J > 0$ for production, the solution for $w > 0$ (upwelling) is:

$$\Delta C = \Delta C_\infty + \left(\frac{J_0}{D\alpha(\alpha - w/D_a)} - \Delta C_\infty\right) e^{-(wz/D_a)} - \left(\frac{J_0}{D_a\alpha(\alpha - w/D_a)}\right) e^{-\alpha z} \qquad (10)$$

where $\Delta C_\infty = C_\infty - C_0$. This is essentially the solution given by Wyrtki [29], except that his production term (R) is positive for consumption. For downwelling ($w < 0$), the boundary conditions are the same, but the preexponential in the $e^{-(wz/D)}$ term must equal zero so that C_∞ is finite. Hence for downwelling, the solution is:

$$\Delta C = \Delta C_\infty - \frac{J_0 e^{-\alpha z}}{D_a\alpha(\alpha - w/D_a)} \qquad (11)$$

According to these equations, downwelling will not change the characteristic distance over which an asymptote is approached for a nutrient profile, but will result in a different asymptotic value. Upwelling will change the shape, and may produce a maximum if ΔC_∞ is low and if production is sufficiently rapid.

In areas of the deep sea where pore water chemistry of oxic sediments has been studied extensively (e.g. Grundmanis et al. [3], and Sites II and IV of this work), little variation has been found in pore water profiles for bioactive elements such as NO_3^- and SiO_2. This is presumably a reflection of the relative constancy over the site of the accumulation rates of organic matter, biogenic silica and inert sedimentary components. Our argument below assumes that, in the absence of advection, nutrient profiles at Site III would also show little variation.

At this site, NO_3^- and SiO_2 profiles may be divided into three groups (Fig. 5). For HP 10 and HP 11, in an intermediate heat flow zone, the profiles are apparently normal diagenetic profiles, while e-folding (or α) values and asymptotes for both NO_3^- and SiO_2 similar to values obtained at our other study sites. NO_3^--depth and SiO_2-depth plots for HP 13 and HP 15, taken in the zone of much higher heat flow, are dramatically distinguished from those of HP 10, HP 11, and HP 14 by being enriched in dissolved SiO_2 and depleted in NO_3^-. The differences are illustrated by comparing NO_3^- and SiO_2 concentrations below 50 cm depth. For all samples in the traverse

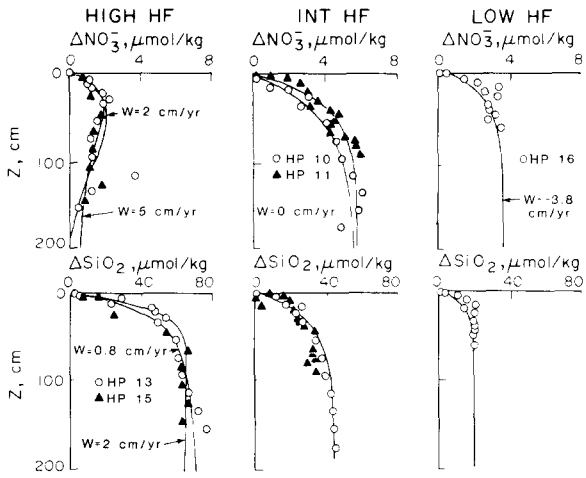

Fig. 5. $\Delta[NO_3^-]$ and $\Delta[SiO_2]$ profiles for Site III. Heat flow is high at the locations of HP 13 and 15 (suggesting upwelling), very low at the location of HP 16 (suggesting downwelling), and intermediate at the location of HP 10 and 11 (suggesting no flow). For the high heat flow profiles (left), the two lines are predicted NO_3^- vs. depth curves and SiO_2 vs. depth curves for indicated values of upwelling rates (in cm/yr), and representative values of α, J_0/D, and ΔC_∞ (SiO_2: $\alpha = 0.0465$, $J_0/D = -0.085$, $\Delta C_\infty = 64$ or 72 μmol/kg; NO_3^-: $\alpha = 0.0211$, $J_0/D = -0.0026$, $\Delta C_\infty = 0.5$ or -0.8 μmol/kg). For the intermediate heat flow profiles (center), the SiO_2 and two NO_3^- curves are for best-fit values of α and ΔC_∞, assuming no advection (NO_3^-: $\alpha = 0.021$ (HP 10) or 0.032 (HP 11), $J_0/D = -0.0026$ (HP 10) or -0.0061 (HP 11), $\Delta C_\infty = 5.88$; SiO_2: $\alpha = 0.0307$, $J_0/D = -0.042$, and $\Delta C_\infty = 46$). For the low heat flow profiles (right), the curves are calculated for $w = -3.8$ cm/yr (downwelling), and representative values of α, J_0/D, and ΔC_∞ (NO_3^-: $\alpha = 0.032$, $J_0/D = -0.0061$, $\Delta C_\infty = 3.8$; SiO_2: $\alpha = -0.0622$, $J_0/D = -0.128$, $\Delta C_\infty = 20$).

(Sites II, III, and IV) excluding those from HP 13, 15 and 16, $\Delta[NO_3^-]$ averages 4.3 ± 1.1 μmol/kg (1σ, $n = 75$) and $\Delta[SiO_2]$ averages 33 ± 10 ($n = 76$). For HP 13 and 15, $[NO_3^-]$ and $[SiO_2]$ means are 1.3 ± 0.4 ($n = 10$) and 67 ± 5 ($n = 11$) μmol/kg respectively. Anomalous asymptotic $[NO_3^-]$ and $[SiO_2]$ values from Hp 13 and HP 15 are thus about 3 standard deviations different from values in areas free of advection. The difference becomes even more dramatic if the comparison is restricted to non-advective profiles from Site III (HP 10, 11, 14). HP 13 is also distinguished from non-advective profiles by a small NO_3^- maximum at 30 cm. The HP 13 and HP 15 profiles are believed to reflect upward advection of SiO_2-rich, NO_3^--poor interstitial waters.

The $[NO_3^-]$ and $[SiO_2]$ profiles of HP 16 are also distinctive; asymptotic NO_3^- and SiO_2 values are less than those of HP 10, 11 and 14. HP 16 was taken in an area of extremely low heat flow, and the profile is tentatively taken as evidence of downwelling, with the low metabolite concentrations being ascribed to washout downcore.

Equations (10) and (11), along with pore water NO_3^- and SiO_2 data, are used to calculate rates of upwelling in HP 13 and 15 and downwelling in HP 16. The e-folding values for the production of NO_3^- and SiO_2 are taken from the fitting of "normal" diagenetic profiles, assuming no advection (HP 10 and 11). ΔC_∞ is estimated visually. For HP 13 and 15, the upwelling rate is calculated by least squares fitting to equation (11). For HP 16, the downwelling rate is calculated from the asymptotic concentration, using equation (11) simplified for $z = \infty$. Best fit curves for NO_3^- and SiO_2 profiles from HP 13 and 15 give upwelling rates of 5 and 1.2 cm/yr respectively, as illustrated in Fig. 5. Also shown are downwelling curves for HP 16 and fits for diagenetic modeling (using equation (1)) for the non-upwelling cases (HP 10 and 11).

Reasonable agreement between the data and the model NO_3^- and SiO_2 profiles for harpoons 13 and 15 support our inference of advection, but there is disagreement between the advection rates calculated for NO_3^- and SiO_2. Tests we have done show that best fit values of w are sensitive to the choice of values for asymptotic concentration (ΔC_∞), but insensitive to the choice of α and J_0/D values. Good fits for the NO_3^--depth and SiO_2-depth profiles from HP 13 and HP 15 are obtained for $w = 2$ cm/yr (Fig. 5), given the plausible ΔC_∞ values of 64 μmol/kg for SiO_2 and -0.8 μmol/kg for NO_3^- (the negative ΔC_∞ value indicates that the $[NO_3^-]$ in the upwelling solutions is less than the bottom water value). We conservatively interpret the data as indicating advection rates at the sites of HP 13 and 15 in the range $+1$ to $+5$ cm/yr, and at the location of HP 16 in the range of -1 to -5 cm/yr.

It is of interest to examine whether the composition of upwelling pore waters sampled by HP 13 and HP 15 has been detectably altered by seawater-basalt reactions. We therefore analyzed samples for Mg^{2+}, Ca^{2+}, and F^-, since those ions are known to behave non-conservatively during water/rock reactions. Within out analytical errors,

TABLE 4

Average concentrations ($\pm 1\sigma$) of Ca^{2+}, Mg^{2+} and F^- in all harpoon samples penetrating the sediment

Site/ harpoon	Number of samples	$[Ca^{2+}]$ (mmol/kg)	$[Mg^{2+}]$ (mmol/kg)	$[F^-]$ (mmol/kg)
II-7	16	10.25 ± 0.10	51.6 ± 0.6	82 ± 15
II-8	7	10.23 ± 0.05		71 ± 3
II-9	12	10.27 ± 0.15		75 ± 7
III-10	14	10.30 ± 0.09		
III-11	16	10.28 ± 0.05		64 ± 4
III-13	13	10.37 ± 0.06	52.4 ± 0.6	67 ± 3
III-14	15	10.44 ± 0.13		67 ± 2
III-15	9	10.31 ± 0.06	53.3 ± 1.0	69 ± 1
III-16	11	10.24 ± 0.10		69 ± 2
IV-17	16	10.66 ± 0.29	52.1 ± 0.3	67 ± 4
IV-18	14	10.47 ± 0.10		60 ± 3
IV-19	20	10.34 ± 0.09		67 ± 1
IV-20	18	10.28 ± 0.09		67 ± 2
IV-21	15	10.31 ± 0.07		
IV-22	14	10.52 ± 0.21		
Seawater		10.25 ± 0.15 ($n = 71$)	52.4 ± 0.5 ($n = 10$)	69 ± 3 ($n = 19$)

the Ca^{2+}, Mg^{2+} and F^- concentrations of HP 13 and HP 15 pore waters are identical to those in the intermediate- and low-heat flow harpoons taken at Site III (Table 4), and $[Ca^{2+}]$ and $[Mg^{2+}]$ are within the range of typical marine pore water compositions observed by Sayles [25]. Apparently convecting seawater is in contact with basalt for too short a time and at too low a temperature for detectable chemical exchange to occur.

Finally, the absence of changes in Ca^{2+}, Mg^{2+} and F^- concentrations underscores the fact that the pore water data standing alone do not provide unequivocal evidence for convection in sediments. The NO_3^- profiles for HP 13 and HP 15 could be explained by invoking a very high C/N ratio in the organic matter being oxidized, along with denitrification near the sediment-water interface. The SiO_2 profiles can be explained by invoking locally high dissolution rates. However, we believe that the topographic, heat flow, and pore water evidence all taken together point strongly to convection through sediments as the cause of high heat flow and anomalous pore water concentrations.

The model of crustal cooling by seawater convection would suggest that the easternmost area studied on the transect, Site IV on 2.5 Myr crust, would be more likely to have thermally driven seawater circulation than Site III because of its youth and its warmer crustal temperatures. There was no evidence of sediment cover on the abyssal hill ridges at Site IV, however, and it is likely that the abundant outcrops on the ridges provide many conduits for ridge flank hydrothermal flow. Thus while it is most likely that convection is occurring at this site, we believe that discharging solutions exit from basement directly into seawater, rather than advecting through sediments.

6. Summary

Both organic matter diagenesis and convection influence pore water chemistry on the western flank of the East Pacific Rise at 20°S. Pore water gradients in areas apparently free of convection have been interpreted in terms of a stoichiometric model. The results suggest a C/N ratio of 106/6.6 at Sites II, III and IV, and C/P ratios of 106/0.24 and 106/0.7 at Sites III and IV, respectively. Except for PO_4^{3-} at Site IV, the organic matter being degraded integrally within the sediments is obviously nutrient-poor relative to the Redfield stoichiometry. Below the sediment-water interface, TA increases with depth due to metabolic CO_2 and NO_3^- production and consequent $CaCO_3$ dissolution, as predicted by stoichiometry. There is however an additional TA increase which, according to the model, would not occur if the pore waters were saturated with respect to calcite. The origin of this excess TA, which appears at the surface but is present down to at least 1 m, is unknown.

At Site III on 4.6 Myr old crust, there is strong evidence from heat flow and pore water chemistry for both upwelling and downwelling zones, with rates ranging from 1 to 5 cm/yr. Ca^{2+}, Mg^{2+} and F^- concentrations in upwelling pore waters are similar to seawater values, suggesting minimal water/rock exchange during convection at these sites.

Acknowledgements

We appreciate the help of Peter Lonsdale, Chief Scientist, and other participants of Ariadne Leg II. We benefitted from discussions with Michael Hobart and his collaborators on their heat flow

results, and permission to summarize their Site III data. It is a pleasure to acknowledge the help of Skip Gleason, whose assistance was essential to many aspects of the field navigation and sampling efforts. This work was supported by a Site Survey Grant from JOI, Inc.

References

[1] P.N. Froelich, G.P. Klinkhammer, M.L. Bender, N.A. Luedtke, G.R. Heath, D. Cullen, P. Dauphin, D. Hammond, B. Hartman and V. Maynard, Early oxidation of organic matter in pelagic sediments of the Eastern equatorial Atlantic: suboxic diagenesis, Geochim. Cosmochim. Acta 43, 1075–1090, 1979.

[2] S.R. Emerson, R. Jahnke, M. Bender, P. Froelich, G. Klinkhammer, C. Bowser and G. Setlock, Early diagenesis in sediments from the Eastern Equatorial Pacific, 1. Pore water nutrient and carbonate results, Earth Planet. Sci. Lett. 49, 57–80, 1980.

[3] V. Grundmanis and J.W. Murray, Aerobic respiration in pelagic marine sediments, Geochim. Cosmochim. Acta 46, 1101–1120, 1982.

[4] S.R. Emerson, V. Grundmanis and D. Graham, Carbonate chemistry in marine pore waters: MANOP sites C and S, Earth Planet. Sci. Lett. 61, 220–232, 1982.

[5] R.N. Anderson and J.N. Skilbeck, Oceanic heat flow, in: The Sea, Vol. VII, Cesare Emiliani, ed., pp. 489–523, John Wiley, New York, N.Y., 1981.

[6] C. Maris, M. Bender, P. Froelich, R. Barnes and N. Luedtke, Chemical evidence for advection of hydrothermal solutions in the sediments of the Galapagos Mounds Hydrothermal Field, Geochim. Cosmochim. Acta 48, 2331–2346, 1984.

[7] R.E. McDuff, Major cation gradients in DSDP interstitial waters: the role of diffusive exchange between seawater and upper oceanic crust, Geochim. Cosmochim. Acta 45, 1705–1713, 1981.

[8] F. Sayles and W. Jenkins, Advection of pore fluids through sediments in the Equatorial East Pacific, Science 217, 245–248, 1982.

[9] M.A. Hobart, D.H. Abbott, R.N. Anderson and P.F. Lonsdale, Detailed geothermal surveys on the East Pacific Rise at 19 deg. South, OES 63, 1103, 1982. (abstract).

[10] M. Leinen, Late Pleistocene hydrothermal sedimentation at DSDP Leg 91 "Hydrogeology" site, EOS 63, 1135, 1982 (abstract). M. Leinen, D.K. Rea et al., Initial Reports of the Deep Sea Drilling Project, Vol. 92, (U.S. Government Printing Office, Washington, D.C. (in press).

[11] I. Hanson and D. Jagner, Evaluation of the accuracy of Gran plots by means of computer calculations. Applications to the potentiometric titration of total alkalinity and carbonate content in seawater, Anal. Chim. Acta 65, 363–373, 1973.

[12] S. Tsunogai, M. Nishimura and S. Nakaya, Complexometric titration of calcium in the presence of large amounts of magnesium, Talanta 15, 385–390, 1968.

[13] J.M. Gieskes, Interstitial water studies, Leg 15, alkalinity, pH, Mg, Ca, Si, and NH_4, in: Initial Reports of the Deep Sea Drilling Project, Vol. 20, pp. 813–829, U.S. Government Printing Office, Washington, D.C., 1973.

[14] R. Greenhalgh and J.P. Riley, The determination of fluorides in natural waters, with particular reference to seawater, Anal. Chim. Acta 25, 179–188, 1961.

[15] J.W. Murray, P. Morrison, K. Krogslund and R. Horowitz, Hydrographic and nutrient data collected during R/V "Thompson" cruise TT154 (15 deg. South), Dep. Oceanogr., Univ. Washington, Spec. Rep. 97, 85 pp., 1981.

[16] F. Goloway and M.L. Bender, Diagenetic models of interstitial nitrate profiles in deep sea suboxic sediments, Limnol. Oceanogr. 24, 624–638, 1982.

[17] Y.H. Li and S. Gregory, Diffusion of ions in seawater and deep-sea sediments, Geomchim. Cosmochim. Acta 38, 703–714, 1974.

[18] D.M. Himmelblau, Diffusion of dissolved gases in liquids, Chem. Rev. 64, 527–541, 1964.

[19] R.A. Berner, Phosphate removal from seawater by adsorption on volcanogenic ferric oxides, Earth Planet. Sci. Lett. 18, 77–86, 1973.

[20] P.N. Froelich, M.L. Bender, N.A. Luedtke, G.R. Heath and T. DeVries, The marine phosphorus cycle, Am. J. Sci. 282, 474–511, 1982.

[21] M. Leinen and N. Pisias, An objective technique for determining end-member compositions and for partitioning sediments according to their sources, Geomchim. Cosmochim. Acta 48, 47–62, 1984.

[22] T. Takahashi, W.S. Broecker, A.E. Bainbridge and R.F. Weiss, Carbonate chemistry of the Atlantic, Pacific, and Indian Oceans: The results of the GEOSECS Expeditions, 1972–1978, Lamont-Doherty Geol. Obs., Tech. Rep. 1, CU 1–80, 1980.

[23] A. Mucci, The solubility of calcite and aragonite in seawater at various salinities, temperatures and one atmosphere total pressure, Am. J. Sci. 283, 780–799, 1983.

[24] F.J. Millero, The effect of pressure on the solubility of minerals in water and seawater, Geochim. Cosmochim. Acta 46, 11–22, 1982.

[25] F.L. Sayles, The composition and diagenesis of the interstitial solutions, I. Fluxes across the seawater-sediment interface in the Atlantic Ocean, Geochim. Cosmochim. Acta 43, 527–545, 1979.

[26] R. Wollast and R.M. Garrels, Diffusion coefficient of silica in seawater, Nature Phys. Sci. 229, 94, 1970.

[27] R. Jahnke, S.R. Emerson and J.W. Murray, A model of oxygen respiration, denitrification and organic matter remineralization in marine sediments, Limnol. Oceanogr. 27, 610–624, 1982.

[28] R. Jahnke, D. Heggie, S. Emerson and V. Grundmanis, Pore water of the central Pacific Ocean; nutrient results, Earth Planet. Sci. Lett. 61, 233–256, 1982.

[29] K. Wyrtki, The oxygen minimum in relation to ocean circulation, Deep Sea Res. 9, 11–23, 1962.